DQ Admittance Extraction for Inverter-Based Resources

Preprint

Rahul H. Ramakrishna,[1] Zhixin Miao,[1] Lingling Fan,[1] and Shahil Shah[2]

1 University of South Florida
2 National Renewable Energy Laboratory

Presented at the 2023 IEEE Power and Energy Society General Meeting
Orlando, Florida
July 16–20, 2023

NREL is a national laboratory of the U.S. Department of Energy
Office of Energy Efficiency & Renewable Energy
Operated by the Alliance for Sustainable Energy, LLC

This report is available at no cost from the National Renewable Energy Laboratory (NREL) at www.nrel.gov/publications.

Contract No. DE-AC36-08GO28308

Conference Paper
NREL/CP-5D00-85295
July 2023

DQ Admittance Extraction for Inverter-Based Resources

Preprint

Rahul H. Ramakrishna,[1] Zhixin Miao,[1] Lingling Fan,[1] and Shahil Shah[2]

1 University of South Florida
2 National Renewable Energy Laboratory

Suggested Citation
Ramakrishna, Rahul H., Zhixin Miao, Lingling Fan, and Shahil Shah. 2023. *DQ Admittance Extraction for Inverter-Based Resources: Preprint*. Golden, CO: National Renewable Energy Laboratory. NREL/CP-5D00-85295.
https://www.nrel.gov/docs/fy23osti/85295.pdf.

NREL is a national laboratory of the U.S. Department of Energy
Office of Energy Efficiency & Renewable Energy
Operated by the Alliance for Sustainable Energy, LLC

This report is available at no cost from the National Renewable Energy Laboratory (NREL) at www.nrel.gov/publications.

Contract No. DE-AC36-08GO28308

Conference Paper
NREL/CP-5D00-85295
July 2023

National Renewable Energy Laboratory
15013 Denver West Parkway
Golden, CO 80401
303-275-3000 • www.nrel.gov

NOTICE

This work was authored in part by the National Renewable Energy Laboratory, operated by Alliance for Sustainable Energy, LLC, for the U.S. Department of Energy (DOE) under Contract No. DE-AC36-08GO28308. Funding provided in part by the U.S. Department of Energy Office of Energy Efficiency and Renewable Energy Solar Energy Technologies Office through DE-EE-0008771 and the Wind Energy Technologies Office through Contract No. DE-AC36-08GO28308. The views expressed herein do not necessarily represent the views of the DOE or the U.S. Government.

Cover Photos by Dennis Schroeder: (clockwise, left to right) NREL 51934, NREL 45897, NREL 42160, NREL 45891, NREL 48097, NREL 46526.

DQ Admittance Extraction for Inverter-based Resources

Rahul H. Ramakrishna, Zhixin Miao, Lingling Fan
Department of Electrical Engineering
University of South Florida
Tampa, FL 33620, USA
rahul12@usf.edu, zmiao@usf.edu, linglingfan@usf.edu

Shahil Shah
National Renewable Energy Laboratory
Denver, Colorado, USA
shahil.shah@nrel.gov

***Abstract*—The power grid industry is pushing for electromagnetic transient (EMT)-based studies for generation interconnection and planning process due to high penetrations of inverter-based resource (IBRs). Vendor-specific and site-specific black-box IBR models are preferred in those simulation studies. For small-signal analysis, measurement-based admittance models are necessary. In this paper, we demonstrate the extraction of frequency-domain dq frame IBR models. These linear models are specific to operating conditions. We demonstrate two extraction methods: frequency scan and a step response-based method. The latter relies on converting time-domain responses to Laplace-domain expressions via eigensystem realization analysis (ERA). Both can lead to dq admittance representation and the latter is time saving.**

***Index Terms*—admittance model, system Identification, frequency scan, eigensystem realization analysis.**

I. Introduction

The power grid industry is pushing for electromagnetic transient (EMT)-based studies for generation interconnection and planning process due to the high penetration of inverter-based resource (IBRs). Vendor-specific and site-specific black-box IBR models are preferred in those simulation studies. For small-signal analysis, measurement-based admittance models are necessary.

In prior works, impedance model based method has been used to analyze sub-synchronous interaction in wind power plants [1] and synchronous machines [2]. In [3], the closed-loop stability of a multi-converter system, including grid-forming and grid-following converters, is analyzed with the *dq* impedance model. Also, the s-domain admittance-based eigenvalue analysis accurately predicts the system's stability [4].

How to obtain impedance model through measurement has been an important research topic. [5] presents a high-power high-voltage testbed setup used to characterize MW-level IBR dq admittance and the frequency scan results. The frequency scan procedure is to sequentially inject sinusoidal signals with a certain frequency into the *d*-axis and *q*-axis voltage and record the current signals. Fourier transformation is then conducted to obtain the phasors of the harmonic component in the voltage and current. From there, dq admittance can be found.

This project is sponsored partly by DOE SETO through DE-EE-0008771 and partly by DOE WETO through Contract No. DE-AC36-08GO28308.

The same frequency scan method can be applied in the EMT simulation to extract the dq admittance of an IBR from its black-box EMT model. There are ongoing efforts taken by the grid operators to produce those models and conduct impedance-based analysis. In a recent report on sub-synchronous oscillation investigation in West Murray region, AEMO suggests the use of impedance analysis as a long-term solution for subsynchronous oscillation monitoring and prevention [6].

Frequency scan is known to produce accurate frequency responses. The disadvantage is that it is time-consuming since it requires many injection experiments, one frequency at a time. Therefore, in the literature, wide-band signal (instead of single frequency signal) injection methods have been also investigated. In [7], the *dq*-impedance of a three-phase system is measured by applying a chirp signal. Chirp Signal is a sinusoidal wave whose frequency increases linearly over time. Impedance identification via impulse waveforms is also under research. In [8], authors identify that measurements from asymmetric bipolar saw tooth impulse waves offer a better accurate model when compared to the traditional uni-polar triangular impulse. The measurement time for these injection methods is significantly short. But their frequency response models are slightly inaccurate. Most recently, Gaussian pulse signals have been investigated for impedance measurement [9].

Besides impulse signals, step excitation has been used to produce measurement data. Laplace-domain *dq* admittance matrix can also be obtained from transient response data by applying ERA, and Dynamic mode decomposition (DMD [10], [11]. This method has been tested by the authors' group for various applications.

In the current paper, we apply both frequency scan and the step excitation method to further examine the influence of operating condition and control parameters on the dq admittance. This study leads to a thorough comparison of frequency scan and the step excitation method for many possible scenarios. We give a summary of detailed implementation tricks on the step excitation method that can lead to success. Also different from the testbeds modeled in MATLAB/Simscape in [10], the testbed in this paper is built in PSCAD, an EMT environment popularly adopted by the grid industry. To generate data, we have developed Python code to conduct automation and utilized Comtrade data format to collect data

for further analysis. The collected data and the data analytics will be made available to the grid industry through DOE SETO's open energy data (OEDI) initiative.

II. The testbed and the two methods

Here, we identify the *dq*-admittance of the Type-4 wind model in the PSCAD/EMTDC environment [12]. The type4 wind model consists of a grid-side controller which regulates the DC link voltage and AC voltage, and the machine-side controller controls the active power at the wind turbine terminals. Both machine and grid side controllers consist of a current controller in the inner loop. The type-4 wind model is interconnected to the grid through a 230-kV transmission line. Fig. 1 represents the testbed and the voltage injection and current measurement points.

The parameters of the system are given in Table I.

TABLE I: Testbed Parameters

Parameter	Value
Grid Voltage ,Frequency	230 kV, 60 Hz
DC-side Voltage	1.45 kV
L_2, R_2	0.86123 mH, 0.1623 Ω
Transformer (T1), X_{tconv}	0.0025 pu
Transformer (T2), X_{t2}	0.1 pu
L_{conv}	335 μF
L_d, R_d	1.675 mH, 5.99050 Ω
C_f, C_d	93.3942 μF, 46.6746 μF
C_{dc}, R_{dc}	15000 μF, 1.159 Ω
Current (K_{pi},τ_i)	0.5, 0.05
Voltage (K_{piv},τ_{iv})	1, 0.02
PLL (K_{PLL},K_{iPLL})	50, 100
DC-Voltage controller (K_{pdc},τ_{idc})	1, 0.02

A. Frequency Scan

The objective of the frequency scan method is to obtain the *dq* admittance of the system as viewed from the point of injection. Here, we inject the system with a small input voltage perturbation with a particular frequency around the steady-state operating condition. We scan the system over a wide range of frequencies to identify the *dq*-admittance of the system. The four components of the *dq* admittance are Y_{dd}, Y_{dq}, Y_{qd}, and Y_{qq}. The *dq*-admittance is defined as:

$$\begin{aligned} Y_{dd}(f_i) &= \frac{i_d^{(1)}(f_i)}{v_d^{(1)}(f_i)} \quad Y_{dq}(f_i) = \frac{i_d^{(2)}(f_i)}{v_q^{(2)}(f_i)} \\ Y_{qd}(f_i) &= \frac{i_q^{(1)}(f_i)}{v_d^{(1)}(f_i)} \quad Y_{qq}(f_i) = \frac{i_q^{(2)}(f_i)}{v_q^{(2)}(f_i)} \end{aligned} \tag{1}$$

where superscripts (1) and (2) refer to perturbations in the *d* and *q* axes, respectively; f_i is the frequency at which the system is perturbed. We must perform the frequency scan for the *d* and *q* axes separately to calculate the *dq* admittance. We also ensure the system has reached a steady state before each scan for accurate measurements. Hence the frequency scan is time-consuming. Fig. 3 presents the frequency-domain measurements obtained via frequency scan.

B. Step excitation method

In this section, we estimate the s-domain *dq*-admittance of a type-4 wind by applying a step input. The Eigensystem Realization Algorithm (ERA) transforms the measured time-domain data (*dq*-currents) into s-domain expressions [8]. The s-domain *dq* admittance can be expressed as follows:

$$Y_{dq} = \frac{s}{p}\begin{bmatrix} i_d^{(1)}(s) & i_d^{(2)}(s) \\ i_q^{(1)}(s) & i_q^{(2)}(s) \end{bmatrix} \tag{2}$$

where $i_d^{(1)}(s)$, $i_q^{(1)}(s)$, $i_d^{(2)}(s)$ and $i_q^{(2)}(s)$ are the predicted Laplace domain expressions of the current signals and p is the size of perturbation.

We generate the input data for estimation by perturbing the *d*-axis and *q*-axis voltage. First, we apply a 0.02 p.u step change to the *d*-axis voltage and measure the *dq* currents $i_d^{(1)}$ and $i_q^{(1)}$, as shown in Fig. 2. Similarly, we record the currents $i_d^{(2)}$ and $i_q^{(2)}$ for a step change of 0.02 p.u in *q*-axis voltage, as seen in Fig. 2. The superscripts (1) and (2) in Fig. 2 refer to perturbation in the *d* and *q* axis, respectively.

The five implementation techniques are summarized below.

- First, we do not apply step changes to both axes simultaneously. The data to be dealt with are essentially generated from a single event. We also treat the data as autonomous responses due to an initial condition perturbation. Thus, the data to be used should have the starting time right after the perturbation is applied.
- The length of the data also matters. It is suggested that the data should capture all essential dynamics till steady-state is achieved. Overly long-period data populates the data Hankel matrix with information with no value and can reduce the matching in the transient time period.
- Downsampling is necessary. AnThe input data shown in Fig. 2 has a sampling frequency of 20 kHz. The ERA method dealt with data Hankel matrix and applies singular value decomposition. Therefore, a large size Hankel matrix consumes long time to conduct linear algebra. A better approach is to down-sample the input data to be approximately 10 times of the interested frequency range. In this case, 830 Hz sampling frequency is used while our interested dynamics are for subsynchronous region.
- Use of zero-mean time-series data. we observed that the ERA performed very well with zero-mean time-series data. Therefore, we subtract the steady-state values from the input data.
- Selection of the order of the estimated system. The order of the dynamic system is an input parameter for the ERA algorithm. A high order leads to better match, albeit overestimation. Thus, the order should be selected as low as possible with reasonable matching. This matching degree has to be determined based on visual examination based on the interested dynamics.

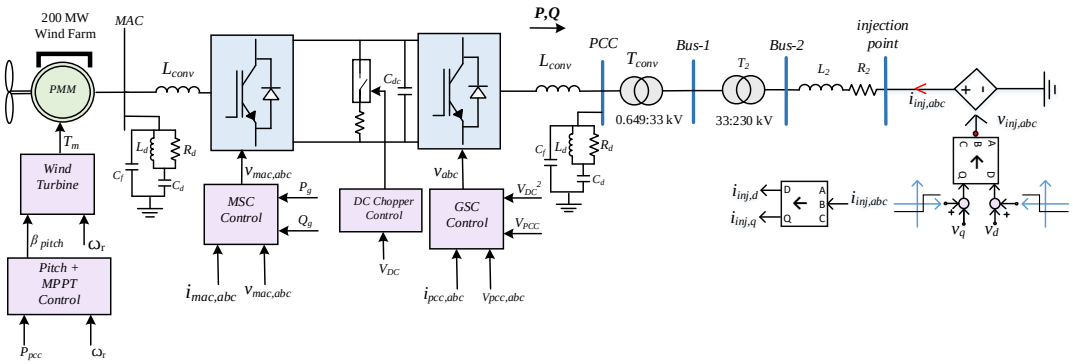

Fig. 1: Type4-wind test bed for frequency scan and step excitation. The grid voltage is perturbed. The current will be recorded and the harmonic component's phasor will be extracted.

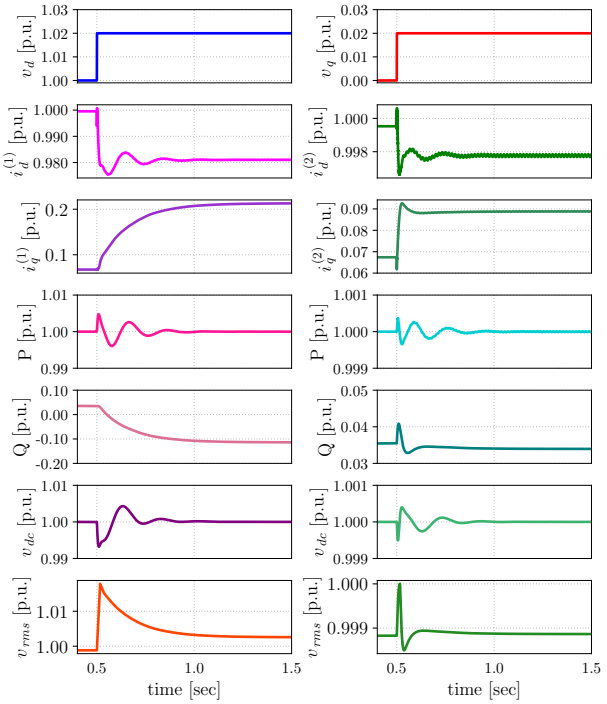

Fig. 2: Input data for estimation with ERA. Left column is obtained by applying a step change to the d-axis voltage only. Right column is obtained by perturbing the q-axis voltage only

The ERA outputs the estimated eigenvalues and residues of the reconstructed signal. Fig. 4 presents the reconstructed signal for a 15$^{\text{th}}$-order approximation of the system. The input data is comparable to the reconstructed signal with excellent match.

We obtain the s-domain expression of the reconstructed signal based on the identified eigenvalues, eigenvectors, and system matrix. Substituting the expression into (2), we get the s-domain dq-admittance model, as shown in Fig. 3. Noticeably, the estimated admittance model is identical to the measured admittance model obtained from the Frequency scan.

We can get better insights into the steady-state operating conditions of the system by evaluating Fig. 3. For $P = 1$ p.u.

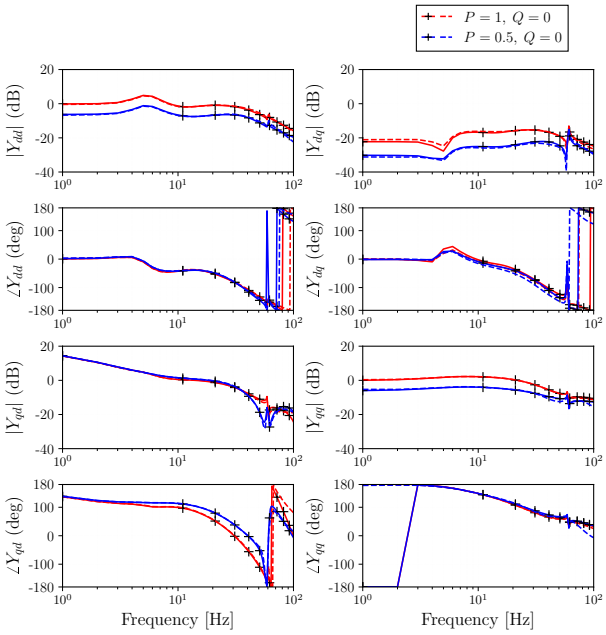

Fig. 3: Comparison of identified dq-admittance model and Frequency-Scan measurements for different operating conditions. Dotted -Line : ERA, Line with Marker : Frequency Scan

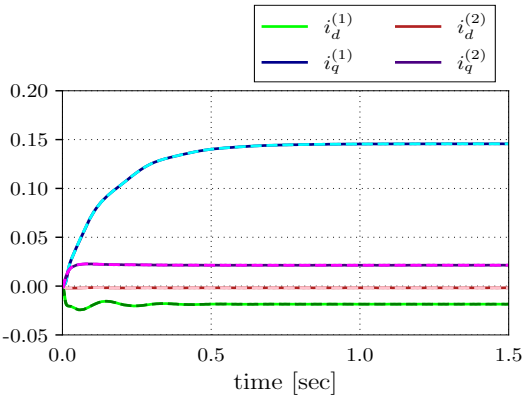

Fig. 4: Comparison of Reconstructed data and input data to the ERA Algorithm. The dotted line represents the Reconstructed signal.

and $Q = 0$ p.u., Y_{dd} and Y_{qq} have a magnitude of 0 dB, which correlates to 1 p.u. Similarly, if $P = 0.5$ p.u. and $Q = 0$ p.u., $|Y_{dd}|$ and $|Y_{qq}|$ are -6.48 dB or 0.4742 p.u. at 0 Hz.

Moreover, 60 Hz in the ABC frame corresponds to 0 Hz in the synchronous frame. Therefore from Fig. 3, we can conclude that magnitude of Y_{dd} and Y_{qq} at low frequency is equal to the steady-state P value. The same observation has been reached for the 2.3-MW inverter with real-power control located in the NREL's Flatrion campus [11]. This observation shows that the low-frequency Y_{dd} when the inverter is in dc-link voltage control has the similar characteristic as the inverter in the real power control.

III. Control Parameters on DQ Admittance

In this section, we further examine control's influence on dq admittance. The dq admittance will be measured by both frequency scan and the step excitation method. The following control bandwidths are examined: dc voltage control, ac voltage control, and inner current control.

1) DC voltage control: In the following subsection, we evaluated the transient performance of the dc-voltage controller. We have presented the *dq*-admittance model of Type-4 wind, as shown in Fig. 5, to illustrate the effect of the DC voltage controller on transient performance. Notably, we have varied the time constant of the DC voltage PI controller and kept the remaining parameters the same, Table I. Fig. 6 presents the simulation results after a step input is applied to the dc-link voltage reference at 0.5 s. Fig. 6 shows that a small time constant leads to fast dc-link voltage track. Furthermore, the dominant dynamic is much faster if the time constant is reduced.

This change of dynamics is also reflected in the dq admittance shown in Fig. 5. It can be seen that Y_{dd}'s peak moved from about 3 Hz to 30 Hz when the time constant reduces from 0.02 s to 0.002 s.

2) AC voltage control: The ac voltage PI controller's integral time constant is varied to test the effect. The time-domain simulation results are presented in Fig. 7. The system reaches steady-state faster when we design the controller with a relatively lower time constant T_i. However, the damping offered by the controller reduces drastically, as shown in Fig. 7. We observe the system has 20-Hz oscillations when we reduce the time constant to 0.004 s.

Fig. 8 shows that the ac voltage controller time constant mainly influences the Y_{qd} component in the subsynchronous frequency region. Fast ac voltage control is reflected as a larger gain in Y_{qd}, which is equivalent to reactive power export and voltage. Therefore, faster voltage control results a tight control of voltage through reactive power injection. On the other hand, if the ac voltage control is too fast, a resonance peak is introduced in all four components, indicating oscillatory issues. Thus, from the frequency response, the time constant

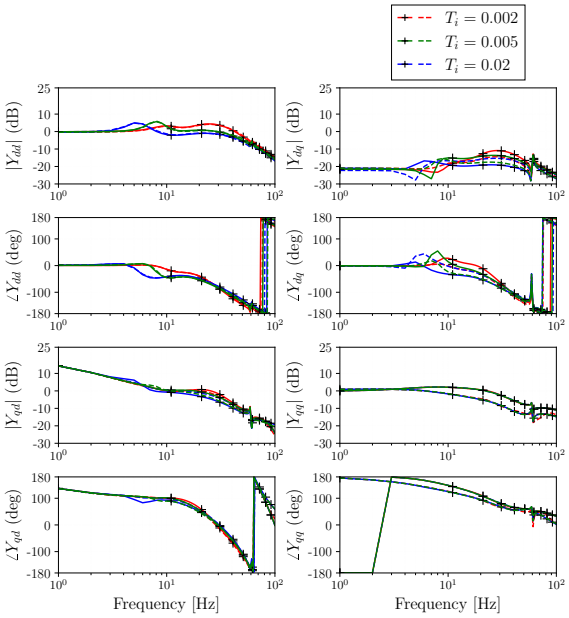

Fig. 5: Effect of the dc voltage control on the dq admittance. Dotted Lines : ERA, Line with Marker : Frequency Scan.

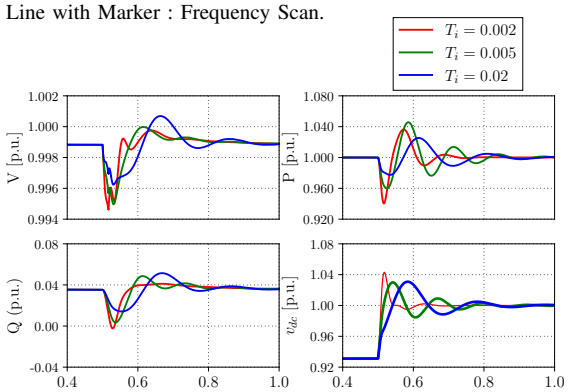

Fig. 6: Transient response of the type-4 wind model for a step change in dc-link voltage order.

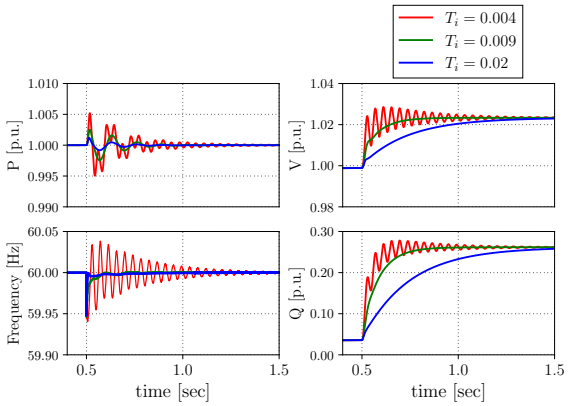

Fig. 7: Transient Response of the type-4 wind model for a 2% step change in AC-voltage

of the ac voltage control cannot be overly small. Resonance peaks should be avoided.

3) Inner current control: In the last experiment, the dc voltage control time constant and ac voltage control time

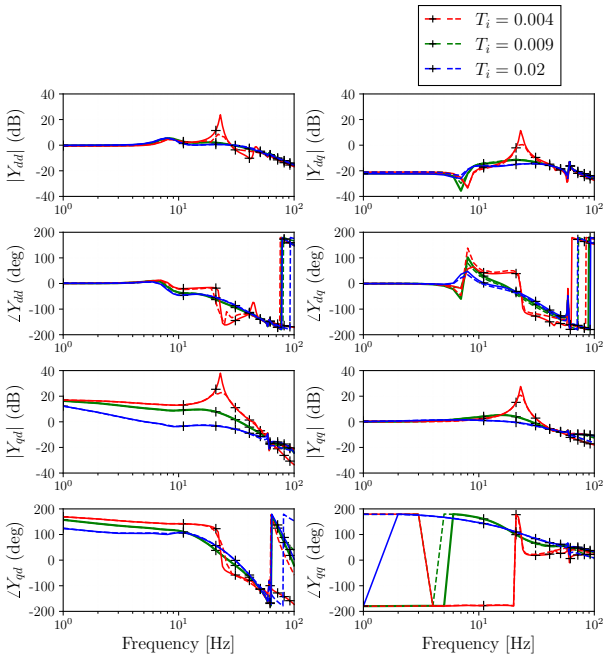

Fig. 8: Influence of ac voltage control parameter on the dq admittance. Dotted Lines : ERA, Line with Marker : Frequency Scan.

constant are selected as 0.002 s and 0.004 s. This set of parameters will lead to the peak at 20 Hz if the inner current control time constant is 0.05 s. To avoid the peak, the inner current control PI controller's integral time constant is reduced to test the effect. Fig. 9 presents the dq admittance. It can be seen that reducing the time constant of the current controller can effectively avoid the peak. Thus, it can be seen that the resonance peak is caused by the interaction of the fast ac voltage control and the slow current control. If their bandwidths are separated sufficiently, resonance peaks are avoidable.

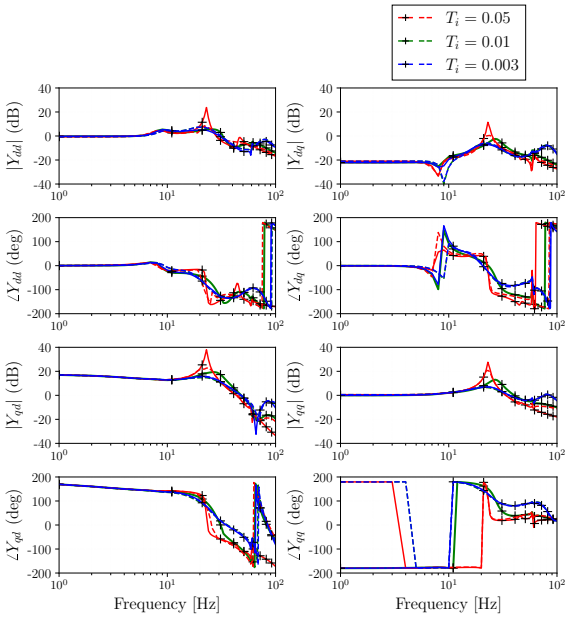

Fig. 9: Influence of inner current control parameter on the dq admittance. Dotted Lines : ERA, Line with Marker : Frequency Scan.

IV. Conclusion

In this paper, we have conducted dq admittance measurement using both frequency scan and step excitation for an IBR model in PSCAD. This paper further confirms the maturity of the step excitation method. Along with the ERA algorithm, this system identification method leads to accurate dq admittance characterization with good match with the result from frequency scan. The obtained dq admittance is in the range of 1 Hz to 100 Hz and the data used for ERA have a length of 1.5 seconds with a sampling frequency at 830 Hz. Furthermore, we have shown the influence of controls on the dq admittance. Dc voltage control changes the Y_{dd} while ac voltage control mainly influences Y_{qd}. Furthermore, if the dq admittance components show a peak in their magnitudes, this peak indicates oscillatory behavior in time domain and should be avoided.

References

[1] B. Badrzadeh, M. Sahni, Y. Zhou, D. Muthumuni, and A. Gole, "General methodology for analysis of sub-synchronous interaction in wind power plants," *IEEE Transactions on Power Systems*, vol. 28, no. 2, pp. 1858–1869, 2013.

[2] B. Agrawal and R. Farmer, "Use of frequency scanning techniques for subsynchronous resonance analysis," *IEEE Transactions on Power Apparatus and Systems*, vol. PAS-98, no. 2, pp. 341–349, 1979.

[3] S. Jiang and G. Konstantinou, "Generalized impedance model and interaction analysis for multiple grid-forming and grid-following converters," *Electric Power Systems Research*, vol. 214, p. 108912, 2023. [Online]. Available: https://www.sciencedirect.com/science/article/pii/S0378779622009634

[4] L. Fan and Z. Miao, "Admittance-based stability analysis: Bode plots, nyquist diagrams or eigenvalue analysis?" *IEEE Transactions on Power Systems*, vol. 35, no. 4, pp. 3312–3315, 2020.

[5] L. Fan, Z. Miao, S. Shah, P. Koralewicz, V. Gevorgian, and J. Fu, "Data-driven dynamic modeling in power systems: A fresh look on inverter-based resource modeling," *IEEE Power and Energy Magazine*, vol. 20, no. 3, pp. 64–76, 2022.

[6] AEMO, "West murray zone sub-synchronous oscillations," 2022.

[7] Z. Shen, M. Jaksic, P. Mattavelli, D. Boroyevich, J. Verhulst, and M. Belkhayat, "Three-phase ac system impedance measurement unit (imu) using chirp signal injection," in *2013 Twenty-Eighth Annual IEEE Applied Power Electronics Conference and Exposition (APEC)*, 2013, pp. 2666–2673.

[8] Z. Liu, J. Liu, and Z. Liu, "Analysis, design, and implementation of impulse-injection-based online grid impedance identification with grid-tied converters," *IEEE Transactions on Power Electronics*, vol. 35, no. 12, pp. 12 959–12 976, 2020.

[9] L. Fan, Z. Miao, L. Bao, S. Shah, and R. H. Ramakrishna, "Dq admittance model extraction for ibrs via gaussian pulse excitation," *under review, IEEE Power Engineering Letters*, 2022.

[10] L. Fan and Z. Miao, "Time-domain measurement-based *dq*-frame admittance model identification for inverter-based resources," *IEEE Transactions on Power Systems*, vol. 36, no. 3, pp. 2211–2221, 2021.

[11] L. Fan, Z. Miao, P. Koralewicz, S. Shah, and V. Gevorgian, "Identifying dq-domain admittance models of a 2.3-mva commercial grid-following inverter via frequency-domain and time-domain data," *IEEE Transactions on Energy Conversion*, vol. 36, no. 3, pp. 2463–2472, 2021.

[12] PSCAD, "Type 4 Wind Turbine Generators," 2018. [Online]. Available: https://www.pscad.com/knowledge-base/article/227